International Journal of Civil Engineering

Soil Mechanics Classic

Antiplane seismic response from semi-sine shaped valley above embedded truncated circular cavity: a time-domain half-plane BEM

M. Panji[1], M. Kamalian[2,*], J. Asgari Marnani[3], M.K. Jafari[4]

Received: February 2013, Revised: November 2013, Accepted: February 2014

Abstract

In this paper, normalized displacement amplitude of the ground surface was presented in the presence of the semi-sine shaped valley above the truncated circular cavity embedded in a homogenous isotopic linear elastic half-plane, subjected to obliquely propagating incident SH waves as Ricker wavelet type. The proposed direct time-domain half-plane boundary element formulation was used and extended to analyze the combined multi-boundary topographic problems. While using it, only boundary of the valley and the surrounding cavity should be discretized. The effect of four geometric parameters including shape ratio of the valley, depth ratio, horizontal location ratio and truncation thickness of the cavity and incident wave angle was investigated on the responses at a single dimensionless frequency. The studies showed that surface behavior was completely different due to complex topographic features, compared with the presence of either valley or cavity alone. In addition, the cavity existence below the surface could play a seismic isolation role in the case of vertical incident waves and vice versa for oblique waves.

Keywords: *Semi-sine shaped valley, Truncated circular cavity, Half-plane BEM, Time-domain, SH-wave.*

1. Introduction

Recent earthquakes have shown that many factors affect ground surface response, among which effects of wave source, path of wave motion and site conditions can be pointed out. In this regard, site effects and status of surface and subsurface roughness are always of the most important factors in the formation of different patterns of ground response. Therefore, better and simpler modeling of topography effects can be extremely affected by identifying the exact behavior of ground surface.

In the literature, different methods are available for preparing surface/subsurface topographic feature models such as analytical, semi-analytical and numerical ones [1].

Among the analytical works, Lee and Trifunac [2] presented an exact solution in terms of cylindrical wave functions to analyze the ground response due to embedded lined circular cavity. Using method of matched asymptotic expansion, Datta and Shah [3] showed free-surface response in the presence of buried circular cavities. Manoogian and Lee [4] and Manoogian [5] applied weighted residual method to the problem of diffraction of SH waves by subsurface arbitrarily shaped inclusions and lined cavities, respectively. One of the few studies in which a close-form solution was presented for the composed topographies was the studies by Lee et al. [6]. They were able to propose an exact analytic series solution for a semi-circle canyon above a subsurface unlined circular cavity. In the work by Smerzini et al. [7], an analytical solution was obtained to determine the response of embedded lined/unlined circular cavity and inclusion. These researchers used expansion of wave functions in terms Bessel and Hankel functions and asked the assistance of Graf's addition theorem to satisfy their boundary conditions. Among the recent works, studies by Tsaur and Chang [8] can be also referred to. They derived a series solution to the SH wave scattering problem of an embedded truncated circular cavity using the region-matching technique.

Despite high accuracy of the analytical and semi-analytical methods because of non-extension to modeling of complex geometric problems, nowadays numerical methods have been widely used. To analyze the seismic behavior of topographic features and solve the wave scattering problems using numerical methods, it is possible

** Corresponding author: Kamalian@iiees.ac.ir*
1 Department of Civil Engineering, Zanjan Branch, Islamic Azad University, Zanjan, IRAN
2 Associate Professor, Geotechnical Engineering Research Center, International Institute of Earthquake Engineering and Seismology (IIEES), No. 26, Arghavan Street, North Dibajee, Farmanieh, Tehran, IRAN
3 Assistant Professor, Civil Engineering Department, Technical and Engineering Faculty, Central Tehran Branch, Islamic Azad University, Tehran, IRAN
4 Professor, Geotechnical Engineering Research Centre, International Institute of Earthquake Engineering and Seismology (IIEES), No. 26, Arghavan Street, North Dibajee, Farmanieh, Tehran, IRAN

to use volumetric and boundary methods. In the volumetric methods such as finite element method (FEM) and finite difference method (FDM), discretizing the whole considered domain including inner and boundary of the body is required. Also, it is needed to define boundaries as energy absorber boundaries to satisfy radiation conditions of waves at infinite boundaries. These agents not only complicate the problem but also increase data volume and analysis time. On the other hand, due to reducing one dimension in the modeling and automatically satisfying the radiation conditions of waves in the basic formulation, boundary element method (BEM) is an appropriate and good method, especially for modeling infinite and semi-infinite continuous media [9, 10].

Although it is possible to use BEM in the time and frequency domain, combining with other volumetric methods and seismic analysis of nonlinear media, dynamic analysis of various problems including time-dependent geometry and determining real-valued results can be only obtained by step-by-step analysis in the time domain. Among the pioneer researchers, Friedman and Shaw [11] gave the first form of boundary element (BE) formulation in the time domain for two-dimensional antiplane problems. Due to small accuracy of their presented full-plane kernels, they have been scarcely used by other researchers. Mansur and Brebbia [12] and Mansur [13] were able to present the general form of time-domain BE formulation as well as transient full-plane displacement and traction kernels for antiplane elastodynamic problems for the first time. Because the Heaviside function was considered in the extracted BE formulation, their kernels were proposed in terms of different states of wave front so that later Dominguez [14] displayed a better view of them by improving basic mathematics of Mansur's kernels. Regardless of Heaviside functions and assuming linear time shape functions at each time step, Israil and Banerjee [15] showed more compact and simpler form of transient full-plane kernels of scalar wave equation. As first researchers, Kamalian et al. [16] modified the transient elastodynamic full-plane kernels of Israil and Banerjee [15] and used them in time-domain BEM algorithm to analyze the site response. Recently, Yu et al. [17] and Soares and Mansur [18] improved the time-domain BEM formulation for scalar wave equation and analyzed various problems with better accuracy.

The previous paragraphs described the development of time-domain BEM based on full-plane fundamental solution or full-plane kernels. If this type of formulation is used to prepare the topographic feature models, then, the smooth ground surface is needed to be discretized to distances too far away from the interested zone. Also, in order to avoid singularity problems in the numerical integration process, it is necessary to close the domain by defining a set of virtual boundary called "enclosing elements" [19]. According to this modeling procedure, several authors elaborated on numerical models of topographic features and analyzed them. Using frequency-domain full-plane BEM, Sanchez-sesma and Campillo [20] and Dravinski [21] analyzed the surface topography including various types of valley and hill. Yu and Dravinski [22] investigated the effects of subsurface inclusions and cavities containing corrugated interface on the smooth ground surface response in the frequency domain. In the time-domain, Takemia and Fujiwara [23] and Kamalian et al. [24-27] were able to use the full-plane BEM formulation for analysis of arbitrarily shaped canyon and hill features as well. Alielahi et al. [28] developed a time-domain BEM formulation for multi-boundary problems in the full-space media and evaluated effects of an embedded circular cavity on the smooth ground displacements. On the other hand, in the BEM formulation, half-plane fundamental solutions or half-plane kernels could be used instead of full-plane case [29]. Accordingly, the smooth ground surface meshing was removed completely, the boundary condition was satisfied exactly, only the boundary of the surface features and the surrounding subsurface openings was discretized and finally time of analysis and accuracy of results were improved in this regard. Many studies can be found using half-plane BEM formulation in the frequency domain and works of Wong and Gennings [30], Sanchez-sesma and Rosenblueth [31], Ohtsu and Uesugi [32], Reinoso et al. [33] and Ausilio et al. [34] for analysis of surface features and Benites et al. [35] for analysis of subsurface topography can be pointed out. Due to complexity of the half-plane time-domain BEM formulation, few studies can be found in the literature and only works by Hirai [36] and Belytschko and Chang [37] are available for analysis of hallow and alluvial valleys, respectively. Recently, Panji et al. [38] reported elastodynamic antiplane half-plane time-convoluted kernels of scalar wave equation as analytical and implemented them in time-domain BEM algorithm to analyze various types of surface/subsurface topographic features.

A review of literature shows that the presented analytical solutions are for simple and noncomplex topographic models. In addition, many numerical studies have been carried out in the frequency domain for either surface or subsurface topography alone and have not investigated their combined interaction effects on the ground response. Therefore, in this paper, considering a model that is actually more visible in the nature, i.e. a semi-sine shaped valley above an embedded truncated circular cavity, normalized displacement amplitude of ground surface were obtained under obliquely propagating incident SH waves by the developed time-domain half-plane BEM. An extensive parametric study was conducted to determine ground surface displacements by changing geometric characteristics of the model such as shape ratio, depth ratio, horizontal location ratio, truncation thickness ratio as well as incident wave's angle. The main purpose of this manuscript included demonstrating effect mode of the mentioned parameters on changing the ground surface patterns at a fixed frequency and preparing simple models in the use of half-plane BEM formulation for analyzing complex irregular sites.

2. Time-Domain Half-Plane BEM

For propagation of antiplane waves (*SH*-wave) in a homogenous isotopic linear elastic half-plane, the scalar wave equation was as follows [39]:

$$\frac{\partial^2 u(x,y,t)}{\partial x^2}+\frac{\partial^2 u(x,y,t)}{\partial y^2}+b(x,y,t)=\frac{1}{c^2}\frac{\partial^2 u(x,y,t)}{\partial t^2} \quad (1)$$

where $u(x,y,t)$ is out of plane displacement at point (x,y) and current time t, c is shear wave velocity and $b(x,y,t)$ is antiplane body force corresponding to displacement direction. The stress-free condition of smooth ground surface which must be satisfied exactly for actual half-plane problems was as follows:

$$\mu\frac{\partial u(x,y,t)}{\partial n}|_{y=0}\ =\ 0 \quad (2)$$

In which μ and n are the shear modulus and normal vector, respectively, and y denotes vertical coordinate axis along the half-plane depth (Fig. 1).

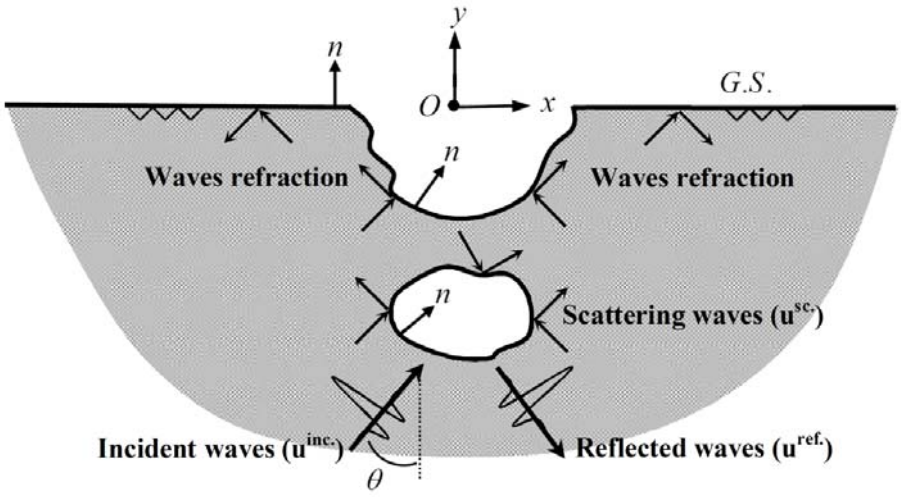

Fig. 1 Waves field for considered combined topographic feature in the current study

After applying weighted residual integral to Eq. (1), removing domain integral statements by boundary methods and ignoring contributions from initial conditions and body forces, the modified boundary integral equation (BIE) for *SH*-wave scattering problem in a half-plane was obtained as follows[14, 32- 33, 40-42]:

$$\begin{aligned} &c(\boldsymbol{\xi})u(\boldsymbol{\xi},t)\\ &=\int_{\Gamma}\left\{\int_0^t [u^*(\boldsymbol{x},t;\boldsymbol{\xi},\tau).q(\boldsymbol{x},\tau)\right.\\ &\left.-q^*(\boldsymbol{x},t;\boldsymbol{\xi},\tau).u(\boldsymbol{x},\tau)]\ d\tau\right\} d\Gamma(\boldsymbol{x})+u^{ff}(\boldsymbol{\xi},t) \end{aligned} \quad (3)$$

In which $u^*(\boldsymbol{x},t;\boldsymbol{\xi},\tau)$ and $q^*(\boldsymbol{x},t;\boldsymbol{\xi},\tau)$ denote transient half-plane displacement and traction fundamental solution in position $\boldsymbol{x}$ and current time t due to a unit antiplane impulsive force in position $\boldsymbol{\xi}$ and preceding time τ, respectively, u and q are boundary displacements and tractions, respectively, $\Gamma(\boldsymbol{x})$ indicates boundary of body, $c(\boldsymbol{\xi})$ is geometry coefficient and $u^{ff}(\boldsymbol{\xi},t)$ denotes free-field displacements which are obtained from the site response without surface or subsurface irregularities. To carry out the analytical temporal integration and numerical spatial integration, after discretizing the time axis by N equal increments with duration Δt ($t=N\,\Delta t$) in the use of linearly shaped functions and meshing the boundary of body by M elements in utilizing the quadratic boundary elements, the above equation can be presented in the following way as a simplified form resulting from eliminating singularity terms from wave fronts:

$$c(\boldsymbol{\xi})u^N(\boldsymbol{\xi})=\sum_{n=1}^{N}\sum_{m=1}^{M}\left[\begin{array}{l}\left\{\int_{\Gamma_m}[U_1^{N-n+1}(\boldsymbol{x}(\kappa),\boldsymbol{\xi})+U_2^{N-n}(\boldsymbol{x}(\kappa),\boldsymbol{\xi})]N_\alpha(\kappa)|J|\,d\kappa\right\}q_\alpha^n-\\ \left\{\int_{\Gamma_m}[Q_1^{N-n+1}(\boldsymbol{x}(\kappa),\boldsymbol{\xi})+Q_2^{N-n}(\boldsymbol{x}(\kappa),\boldsymbol{\xi})]N_\alpha(\kappa)|J|\,d\kappa\right\}u_\alpha^n\end{array}\right]+u^{ff.N}(\boldsymbol{\xi}) \quad (4)$$

where $U_1^{N-n+1}(\boldsymbol{x},\boldsymbol{\xi})+U_2^{N-n}(\boldsymbol{x},\boldsymbol{\xi})$ and $Q_1^{N-n+1}(\boldsymbol{x},\boldsymbol{\xi})+Q_2^{N-n}(\boldsymbol{x},\boldsymbol{\xi})$ denote the half-plane displacement and traction time-convoluted kernels proposed as analytic expressions by Panji *et al.* [38], u^N and $u^{ff.N}$ stand for the boundary and free field displacement at time $t=N\,\Delta t$, respectively, $N_\alpha(\kappa)$ is

quadratic shape functions in terms of local intrinsic coordinates ($\alpha = 1, 2, 3$) and J indicates Jacobian of transformation from Cartesian to local coordinates systems. u^n and q^n are displacements and tractions of boundary, respectively. Γ_m stands for portion of the boundary to which element "m" belongs. After spatial integration of Eq. (4) for each boundary node located on Γ_m, the following equation in the matrix form can be obtained:

$$\sum_{n=1}^{N} \boldsymbol{H}^{N-n+1} \{\boldsymbol{u}^n\} = \sum_{n=1}^{N} \boldsymbol{G}^{N-n+1} \{\boldsymbol{q}^n\} + \{\boldsymbol{u}^{ff.N}\} \quad (5)$$

in which $\boldsymbol{H}^{N-n+1}$ and $\boldsymbol{G}^{N-n+1}$ are the matrices whose elements are determined by integration over the boundary elements, $\{\boldsymbol{u}^n\}$ and $\{\boldsymbol{q}^n\}$ are vectors of boundary nodal quantities at the time step n. This form of Eq. (5) cannot be solved straightforwardly. After applying the boundary conditions specified as known displacement or traction at each boundary node and reordering the matrix columns corresponding to unknown boundary quantities to the left, the soluble form of the above equation was derived as follows:

$$[\boldsymbol{A}_1^1]\{\boldsymbol{X}^N\} = [\boldsymbol{B}_1^1]\{\boldsymbol{Y}^N\} + \{\boldsymbol{R}^N\} + \{\boldsymbol{u}^{ff.N}\} \quad (6)$$

where $\{\boldsymbol{X}^N\}$ and $\{\boldsymbol{Y}^N\}$ are vectors of unknown and known boundary quantities, respectively, $[\boldsymbol{A}_1^1]$ and $[\boldsymbol{B}_1^1]$ are the matrices whose columns are corresponding to unknown and known boundary quantities, respectively, and need to be only computed in the first time step for problems with time independent geometry, $\{\boldsymbol{u}^{ff.N}\}$ is vector of including free field displacements which must be computed in each time step and added to the right hand side of Eq. (6), and $\{\boldsymbol{R}^N\}$ denotes effects of past dynamic history on the current time node N, presented as follows:

$$\{\boldsymbol{R}^N\} = \sum_{n=1}^{N-1} (\boldsymbol{G}^{N-n+1} \{\boldsymbol{q}^n\} - \boldsymbol{H}^{N-n+1} \{\boldsymbol{u}^n\}) \quad (7)$$

After solving Eq. (6) in each time step, all unknown boundary quantities including displacement or traction can be obtained. To determine the response values beyond the valley boundary on the smooth ground surface as internal points, the geometry coefficient $c(\boldsymbol{\xi})$ can be assumed equal to unit in Eq. (3) and the above steps can be repeated.

3. Excitation Waves Type

The type of excitation waves was assumed as the Ricker wavelets according to the following function [40, 43]:

$$f(t) = \left[1 - 2\left(\pi\, f_p (t - t_0)\right)^2\right] e^{-\left(\pi\, f_p (t - t_0)\right)^2} \quad (8)$$

where f_p and t_0 are predominant frequency and time shift parameter, respectively. Considering that antiplane response was desirable, the incidence displacement was *SH*-wave type as follows:

$$u^{inc.}(x, y, t) = a_{max} \,.\, f(\alpha^{inc.})\, H\left(t - \frac{r^{inc.}}{c}\right) \quad (9)$$

in which a_{max} and $H(.)$ indicate the maximum displacement time history and Heaviside function, respectively, and argument $\alpha^{inc.}$ denotes phase of incident waves in location $r^{inc.}$ and time t is to be measured from a specified location in which the origin of coordinates was assumed as in Fig. 1 (point O). To satisfy the boundary condition in Eq. (2), it is necessary to consider a reflected wave field including the reverse phase as follows:

$$u^{ref.}(x, y, t) = a_{max} \,.\, f(\alpha^{ref.})\, H\left(t - \frac{r^{ref.}}{c}\right) \quad (10)$$

where $u^{ref.}(x, y, t)$ is the reflex displacement and $\alpha^{ref.}$ indicates the phase of reflected waves. By adding Eq. (9) and Eq. (10), the free field displacement can be obtained as:

$$u^{ff}(x, y, t) = a_{max} \,.\, \left(\begin{array}{l} \left[1 - 2\left(\frac{\pi\, f_p}{c}\, \alpha^{inc.}\right)^2\right] e^{-\left(\frac{\pi\, f_p}{c} \alpha^{inc.}\right)^2} H\left(t - \frac{r^{inc.}}{c}\right) + \\ \left[1 - 2\left(\frac{\pi\, f_p}{c}\, \alpha^{ref.}\right)^2\right] e^{-\left(\frac{\pi\, f_p}{c} \alpha^{ref.}\right)^2} H\left(t - \frac{r^{ref.}}{c}\right) \end{array} \right) \quad (11)$$

in which:

$$\alpha^{inc.} = c\,(t - t_0) + r^{inc.}; \quad r^{inc.} = -sin\theta.x + cos\theta.y \quad (12)$$

For the incidence wave field and:

$$\alpha^{ref.} = c\,(t - t_0) + r^{ref.}; \quad r^{ref.} = -sin\theta.x - cos\theta.y \quad (13)$$

For the reflected wave filed. θ is the angle of excitation waves as in Fig.1, and (x, y) indicates coordinates of boundary nodes. u^{ff} shown in Eq.(11) must be placed in the left hand side of Eq.(3).

4. Validation Example

The above formulation was implemented in a general time-domain BEM code known as DASBEM (Dynamic Analysis of Structures using Boundary Element Method).

This algorithm is able to analyze all dynamic problems including antiplane seismic evaluation of surface/subsurface topographic features either alone or in combined cases and also cover problems due to external vibrations resulting from arbitrarily functional time-dependent loads. Verifications of DASBEM with those of the published works in the solving of single features such as full/truncated semi-circle valley and full/truncated embedded circular cavity can be found in the work by Panji *et al.* [38]. But, considering that this study was concerned with the investigation of the combined effects of surface and subsurface features, the analytical work of Lee *et al.* [6] was selected as the benchmark. Fig. 2 shows a validation example as well as their discretized zones. As can be observed, a semi-circle valley was located the above the circular cavity embedded in depth of 2.5 b due to obliquely propagating incident *SH* waves. The number of nodes which were defined on the valley, cavity and beyond the valley was equal to 63, 62 and 80, respectively. The time step was selected equal to 0.005 sec. The Ricker wavelet specifications were equal to 3.0 Hz, 2.0 s and 0.001 m for predominant frequency, time shift parameter and maximum amplitude, respectively. The normalized displacement amplitude (the ratio of Fourier amplitude of the total motion obtained by BEM to the Fourier amplitude of the incident motion) of valley surface and its beyond can be observed in Fig. 3 due to incidence wave with angles of 0, 30, 60 and 90 degrees at dimensionless frequency of $12/\pi$ (the dimensionless frequency denoted by $\boldsymbol{\eta}$ is defined as $\omega\, b/\pi\, c$, in which ω presents angular frequency of the wave, b is the radius of canyon and c is the shear wave velocity). As can be seen in Fig. 3, the accuracy of results was favorable and in good agreement with *SH*-wave scattering problem from combined topographic features.

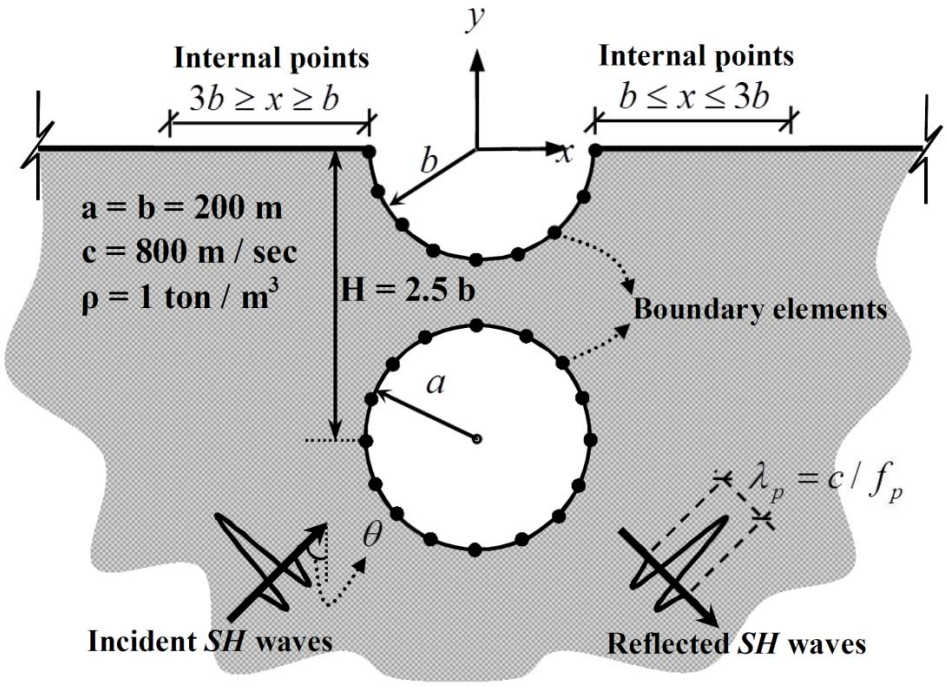

Fig. 2 Schematic half-plane BEM model for the validation example: a semi-circle valley above a subsurface circular cavity in depth of 2.5b subjected to obliquely propagating incident *SH* waves as the Ricker wavelets type

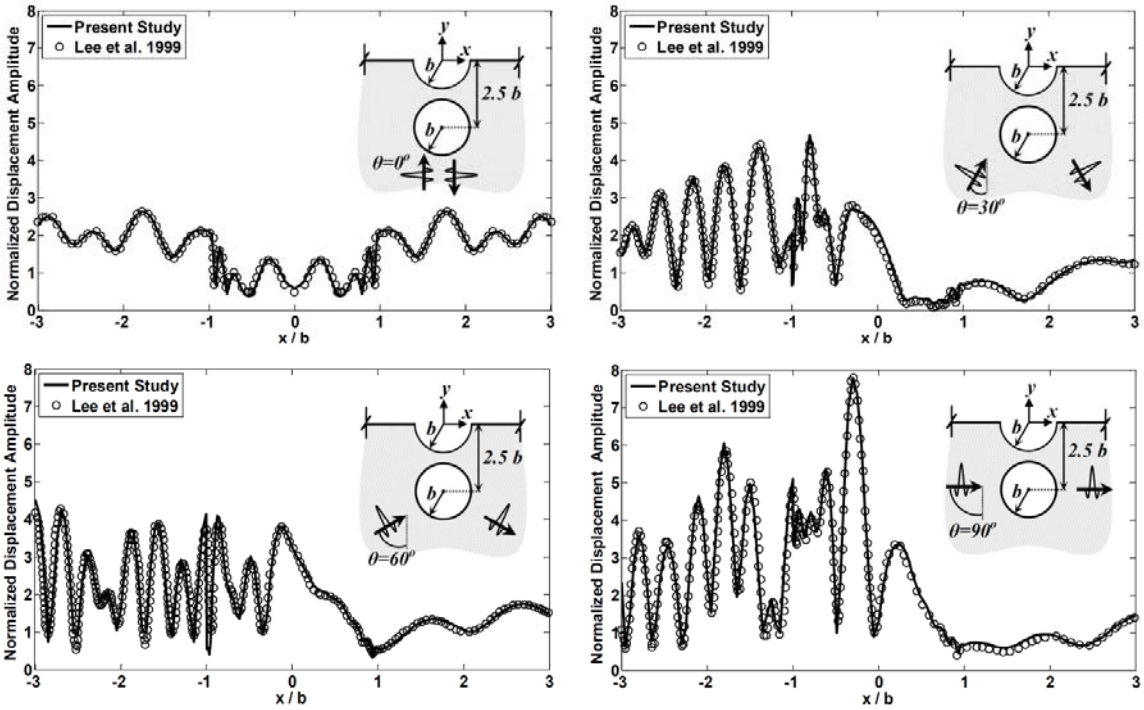

Figure 3. The response of the ground surface in the presence of a semi-circle valley above an embedded circular cavity in depth of 2.0 at dimensionless frequency (η) of 12/π

5. Methodology of the Numerical Study

For a more realistic model of the canyon on the subsurface hole, the semi-sine shaped cross section in accordance with the following function was considered for the valley and a horseshoe-shaped unlined tunnel (truncated circular cavity) embedded beneath it was assumed as in Fig. 4:

$$\zeta(x) = -0.5\,h\left(1+\cos\left(\frac{\pi x}{b}\right)\right) \quad |x| \le b$$
$$\zeta(x) = 0 \quad |x| > b \tag{14}$$

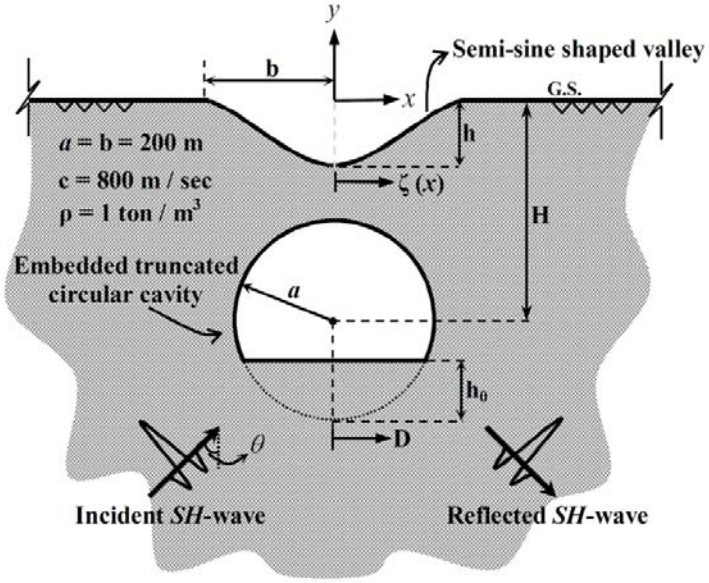

Fig. 4 Schematic model for the numerical study: a semi-sine shaped valley above an embedded truncated circular cavity subjected to obliquely propagating incident *SH* waves as the Ricker wavelets type

where h and b denote depth and half-width of the valley, respectively. In order to carry out parametric studies, four geometrical ratios, namely shape ratio ($SR = h/b$), depth ratio ($DR = H/b$), location ratio ($LR = D/b$) and truncation ratio ($TR = h_0/b$) as well as angle of excitation waves (θ) were investigated to obtain the site response and achieve the normalized displacement amplitude. The values of 0.0, 0.1, 0.3, 0.5 and 1.0 for shape ratio, 2.5, 4.0, 6.0 and 8.0 for depth ratio, 0.0, 2.0, 4.0 and 8.0 for location ratio, 0.0, 0.4, 0.65 and 1.0 for truncation ratio and finally 0.0, 30, 60 and 90 degrees for angle of incident waves were considered. When the effect of these parameters was not evaluated alone, the values of 0.5, 2.5, 0.0 and 0.4 were assumed for ratios of shape, depth, location and truncation, respectively [8, 44]. In all the cases, excitation waves had a predominant frequency equal to 3 Hz and a time shift parameter was considered from 2 to 5 sec depending on the depth and position of the cavity. A uniform discretization was carried out on both surfaces of valley and cavity with the distance of nodes equal to 10 m. In this study, due to the interests of engineering, half-width of the valley was assumed equal to the radius of the cavity ($a = b$) and the results were presented at dimensionless frequency of 2.0 (actual frequency of 4 Hz), approximately corresponding to incident waves with short wavelength [5-6].

Finding the answers for these questions was the main purpose of the numerical study: How could the response of the ground surface in the existence of the valley above the truncated cavity be changed with different shape ratios compared to those of without valley? What is the ground response to changes of the depth and horizontal positions of the truncated cavity compared to the case of non-cavity half-plane? What is the effect on the response patterns due to changes in the cavity section from full-circle to semi-circle? Which angle of incident waves obtains the maximum ground response in a fixed position for combined topographies?

6. General Time-Domain Response

To view general patterns of responses in the time domain, Fig. 5 was presented. In this figure, scattering and diffraction of waves in the presence of a semi-sine shaped valley with $SR = 1.0$ can be observed above an embedded truncated cavity in depth of $2.5b$. The responses were shown in the range of $3b$ to $-3b$ on the ground surface. Despite the responses in the frequency domain, effect of reflection and diffraction of waves can be seen in the time domain.

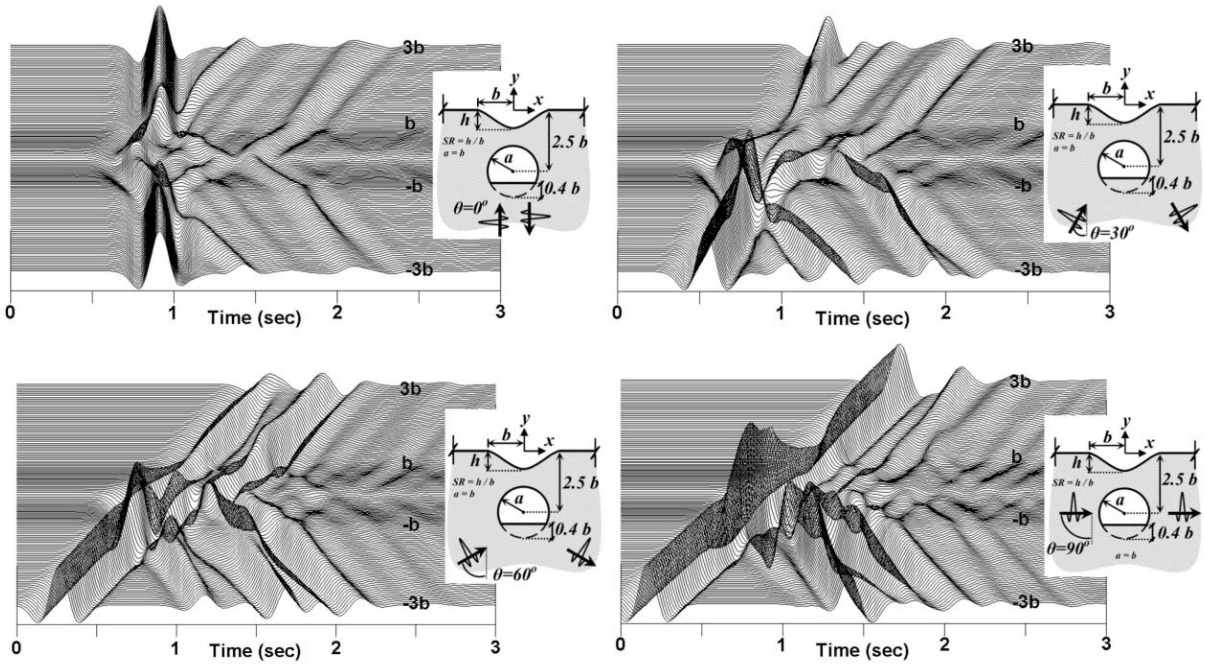

Fig. 5 Time-domain response of the ground surface in the presence of a semi-sine shaped valley with shape ratio equal to 1.0 (SR=1.0) above an embedded truncated circular cavity in depth of 2.5b

As can be seen in Fig. 5, in the case of vertically propagating incident waves, in addition to maintaining the symmetry of responses, small amplitude of displacements existed inside the valley and large amplitudes can be observed in the edges. Considering that the phase difference of the direct and reflected waves from the surface of valley was greater than the smooth ground surface, effects of their separation was clearly specified. However, because of the existence of zero phase difference on the smooth surface, the responses tended to the free-field motion with distance from the valley surface. In general, the type of diffracted waves which seemed to

be started from the edges and propagated on the curvature surface of the valley was called "creeping waves" [40, 45]. Separating the contribution of these waves from total response was difficult. As can be seen, contribution of reflected waves from cavity surface was also found. This type of secondary reflected waves as cascading flow started from the end of primary reflected waves and got away from valley surface with the certain slope due to increase of distance between observation points and source points on the smooth ground and valley surface, respectively.

In the case of inclined waves, the ground behavior left the symmetry state and scattered waves with large amplitude can be seen on the side of near the arrival wave front. It is obvious that, by increasing the angle of incident waves, the response amplitudes increased in the edge of the close to the wave front. Also, the trapped and multiple reflections of waves increased between the valley and cavity surface on that side.

7. Frequency-Domain Response

The general pattern of surface displacement and observing its behavior under seismic forces was only possible in the frequency domain. Fig. 6 was presented for this purpose. In this figure, due to different angles of incident waves, the amplitude of normalized displacements of ground surface in the range of $3b$ to $-3b$ versus dimensionless frequencies was plotted for a valley with $SR = 1.0$ above a truncated circular cavity embedded in depth of $2.5b$. As can be seen, the responses were generally at the valley slopes smaller than its edges. Although increasing the dimensionless frequency (or decreasing the dimensionless period defined as ratio of incident wavelength to total width of the valley) influences on the formation of the responses, it was seen that the amplitudes were not varied very much by changes of the frequency in the vertically incident waves.

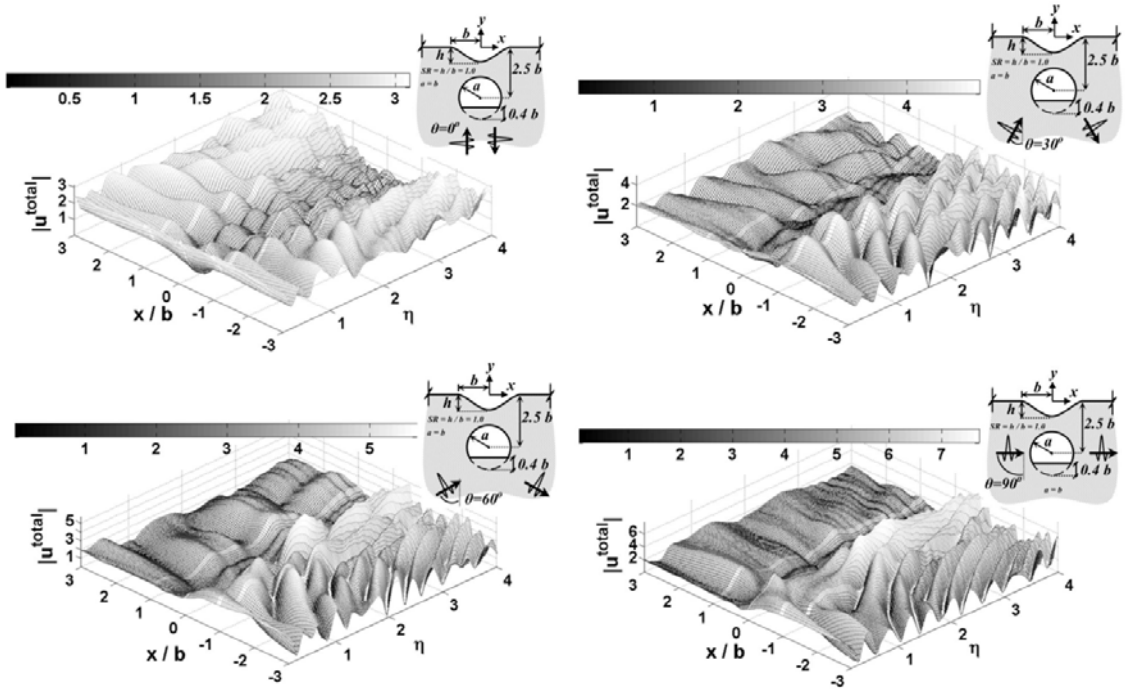

Fig. 6 The response of the ground surface versus different dimensionless frequencies in the presence of a semi-sine shaped valley with SR=1.0 above an embedded truncated circular cavity in depth of 2.5b

In the case of oblique waves, the behavior was completely different. In this case, the maximum responses were observed in the edges near the arrival wave front and fluctuations of response can be also seen on that side. With increasing the angle of incident waves, the amplitude of responses decreased on the side away from the entrance wave front and increased on another side so that the hollow valley and cavity played the role of guard trench against the wave front and did not allow for the waves to have significant impact behind the valley. In other references [46], this effect has been mentioned as "shadow zone", leading to the formation of standing patterns in responses at those points.

7.1. Shape ratio effect

The geometric parameter of valley shape ratio (SR) was studied to see the effect of its height on surface displacements. In Fig. 7, the normalized displacement amplitude of ground surface is shown for different shape ratios of the valley in the presence of a truncated circular cavity embedded in the depth of $2.5b$ at dimensionless frequency of 2.0 under obliquely propagating incident *SH* waves including various angles. As can be observed in the case of vertically propagating waves, the lowering effects (seismic isolation) in the response were specified clearly

due to the cavity existence so that the resulted displacements were small in all shape ratios on the valley surface and its edges compared with the smooth ground surface ($SR = 0.0$). Also, in this case, deepening the valley was not highly affected in the increase of response amplitude on the valley surface and its fluctuations only increased. However, in the case of obliquely propagating waves, isolation effects of cavity decreased on the responses compared to smooth ground so that large displacements were shown on the deep valley in the angles of 60 and 90 degrees. The important point was that the shape ratio effects changed the obtained amplitudes on that side, which was farther away from the arrival wave front.

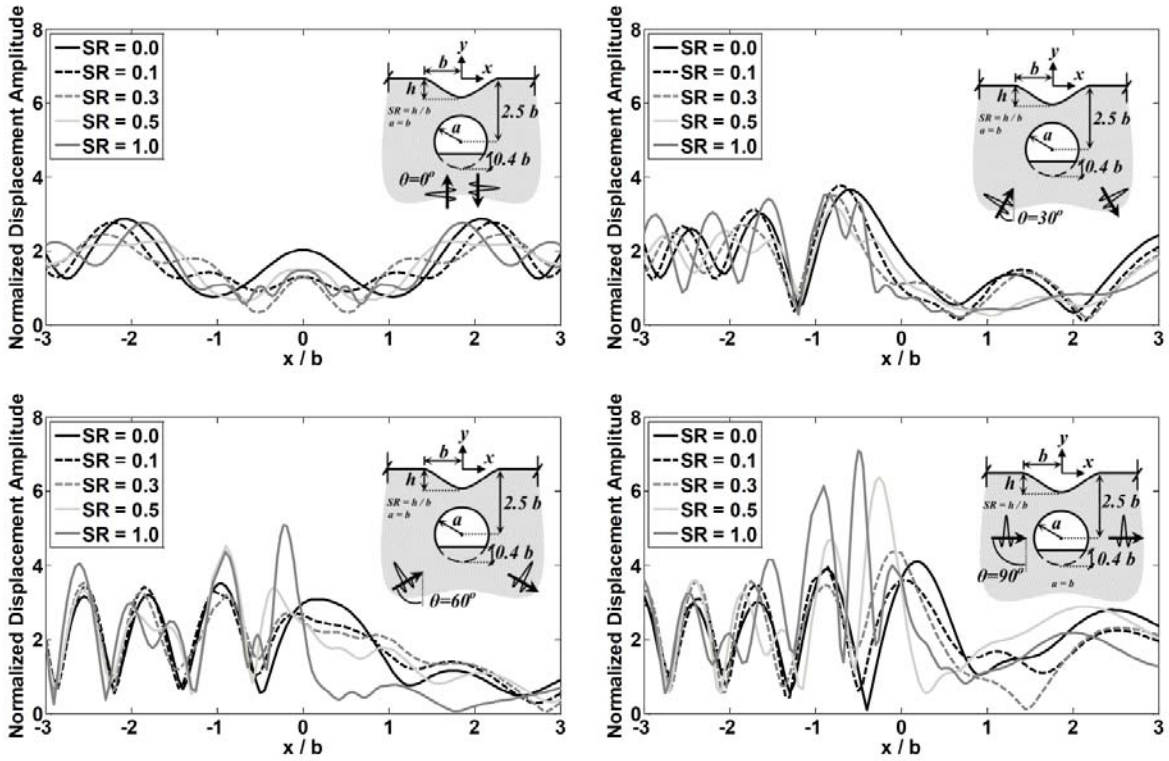

Fig. 7 The effect of the valley shape ratio (SR=h/b) on the response of the ground surface in the presence of an embedded truncated cavity in depth of 2.5b at dimensionless frequency 2.0

7.2. Depth ratio effect

Perhaps, investigation of the cavity depth showed better effect of underground openings on the ground response. In this regard, in Fig 8, the normalized displacement amplitude of the surface was presented for different depth ratios ($DR = H/b$) in the presence of a valley with the shape ratio of 0.5 at dimensionless frequency of 2.0, subjected to obliquely propagating incident *SH* waves. As displayed in the previous section, in the case of vertically propagating waves, existence of the underground cavity had the complete role of seismic isolation so that the responses on the valley increased with increasing the depth of truncated cavity and the maximum response was reserved for a half-plane without embedded hole ($DR = \infty$). Nevertheless, increasing the depth ratio affected the response reduction in the edges near the valley. On the other hand, in the case of inclined waves, the cavity isolation effect was eliminated on decreasing the displacement amplitudes with increasing the incident wave angle, especially on the side of near the arrival wave front, to observe the maximum amplitude on the valley in the smallest depth of the cavity ($DR = 2.5$) for wave angels of 60 and 90 degrees. As can be shown in Fig. 8, for the mentioned wave angles, the responses almost approached the free-field motion on the side near the arrival wave front for a non-hole half-plane case ($DR = \infty$). It should be noted that reduction of the response fluctuations can be always seen with decreasing the wave's angle.

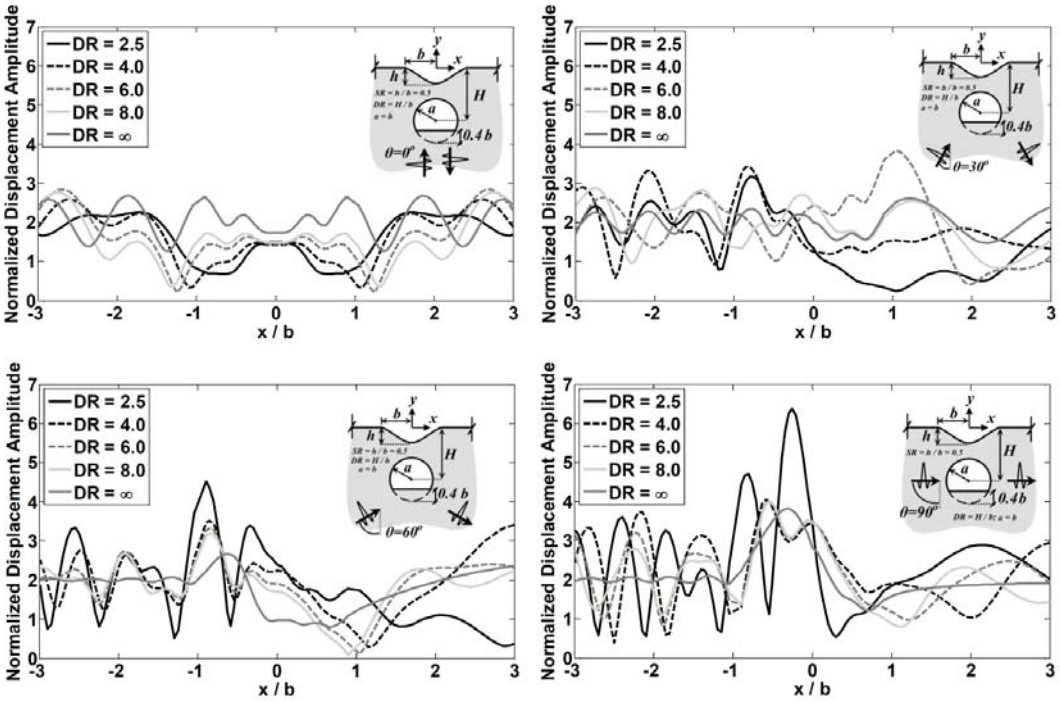

Fig. 8 The effect of the cavity depth ratio (DR=H/b) on the response of the ground surface in the presence of a semi-sine shaped valley with SR=0.5 at dimensionless frequency 2.0

7.3. Location ratio effect

In this section, horizontal location effect of truncated cavity is investigated on the ground surface response in its fixed depth of 2.5b. Fig. 9 shows the normalized displacement amplitude of the valley surface and its beyond with shape ratio of 0.5 in various location ratios ($LR = D/b$) of embedded truncated cavity at dimensionless frequency of 2.0 due to different angles of antiplane seismic incident waves including 0, 30, 60 and 90 degrees.

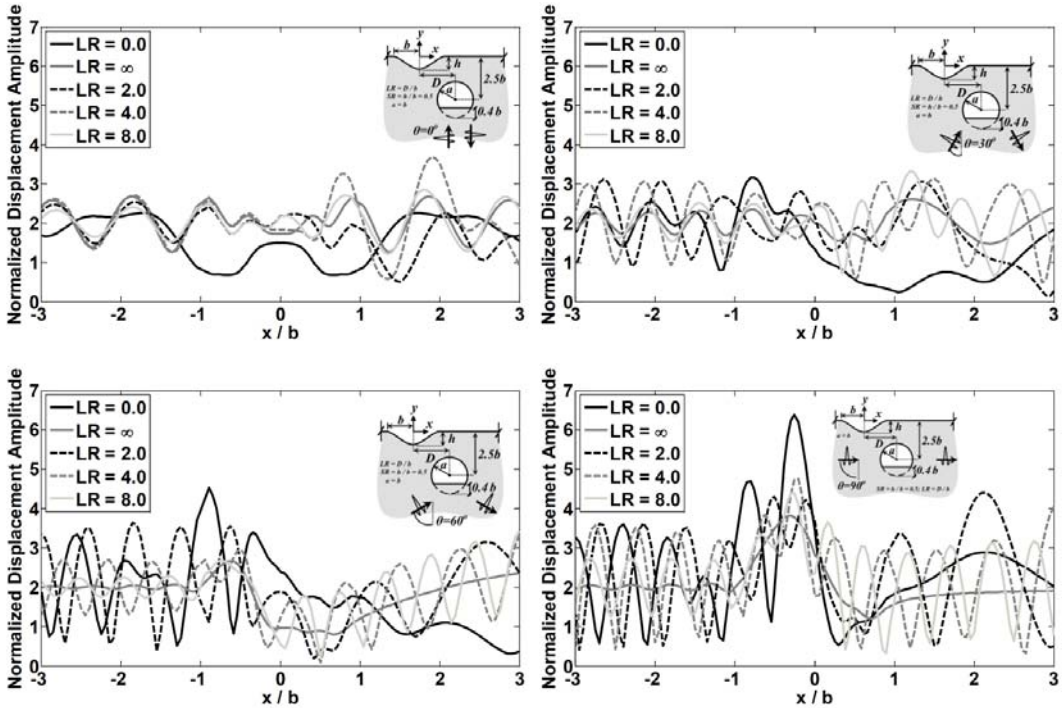

Fig. 9 The effect of the cavity horizontal location ratio (LR=D/b) on the response of the ground surface for DR=2.5 in the presence of a semi-sine shaped valley with SR=0.5 at dimensionless frequency 2.0

As can be seen, in addition to increasing the responses on the valley, they were converged to the answer of non-hole half-plane case ($LR = \infty$) by moving the horizontal location of the cavity in vertically propagating waves. The part of the valley which was close to entrance wave front or, in other words, the part of the valley which was far from the cavity location, was rapidly converged. The low scattering and diffraction of the waves from the cavity crest surface on that side can cause this subject. Although the response fluctuations increased in the case of inclined waves, these oscillations focused on the responses of non-hole half-plane case so that their amplitudes decreased with increasing the location ratio (LR). Unlike the vertical waves, the maximum response on the valley belonged to the case of the cavity without eccentricity ($LR = 0$) for the oblique waves.

7.4. Truncation ratio effect

Fig. 10 shows effect of truncation thickness ratio (TR) of circular cavity on the ground surface response. In this figure, normalized displacement amplitude of the surface was presented in the presence of a valley with shape ratio of 0.5 above a cavity immersed in the depth of 2.5b including different truncation ratios at dimensionless frequency of 2.0 subjected to obliquely propagating incident *SH* waves as 0,30, 60 and 90 degrees. As can be seen, varying the cavity section from full-circle ($TR = 0.0$) to semi-circle ($TR = 1.0$) had little effect on the seismic response of the ground, except a few insignificant changes in the response behavior of that part of the valley which was far away from the arrival wave front.

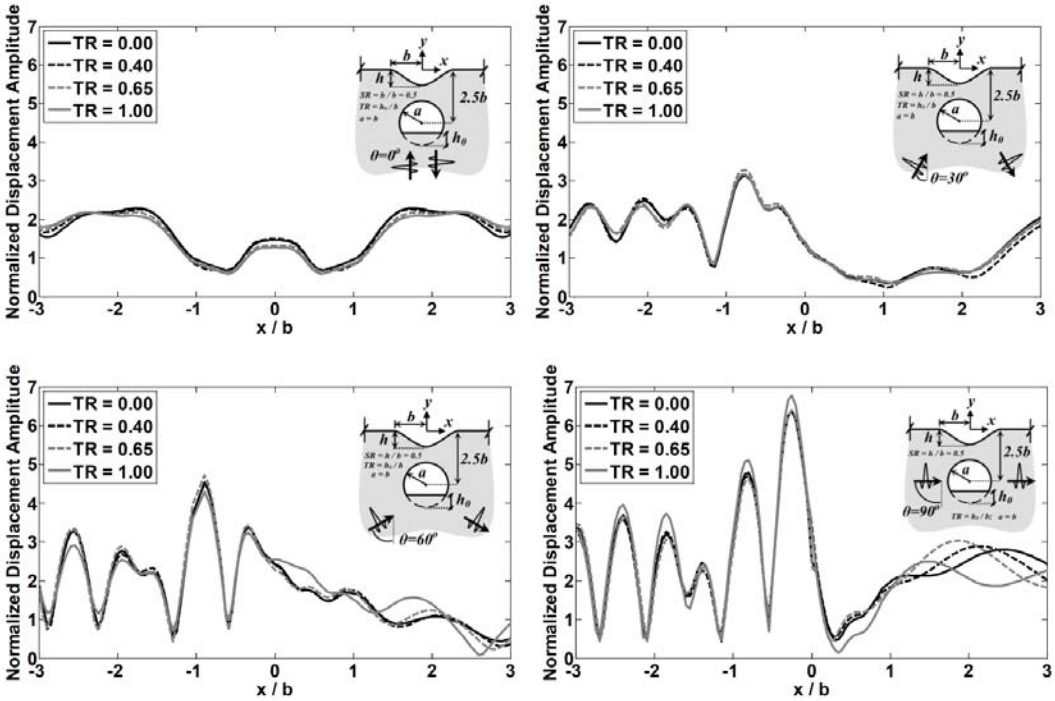

Fig. 10 The effect of the cavity truncation thickness ratio (TR=h_0/b) on the response of the ground surface in the presence of a semi-sine shaped valley with SR=0.5 at dimensionless frequency 2.0

7.5. Wave angle effect

Although the effect of incident wave angle was specified on the antiplane seismic behavior of the surface somehow in all the above figures, Fig. 11 was plotted for precise view of this purpose. The effect of wave angle was demonstrated on the response patterns of the surface for two cases of the titled geometric ratios in the mentioned figure. As can be seen, the wave angle effect was large in the changes of response patterns. In all the cases, the maximum amplitude belonged to incident angle of 90 degrees and was observed in the valley edge near the arrival wave front. Furthermore, the part of the valley which was away from the wave front experienced low fluctuations and little response changes.

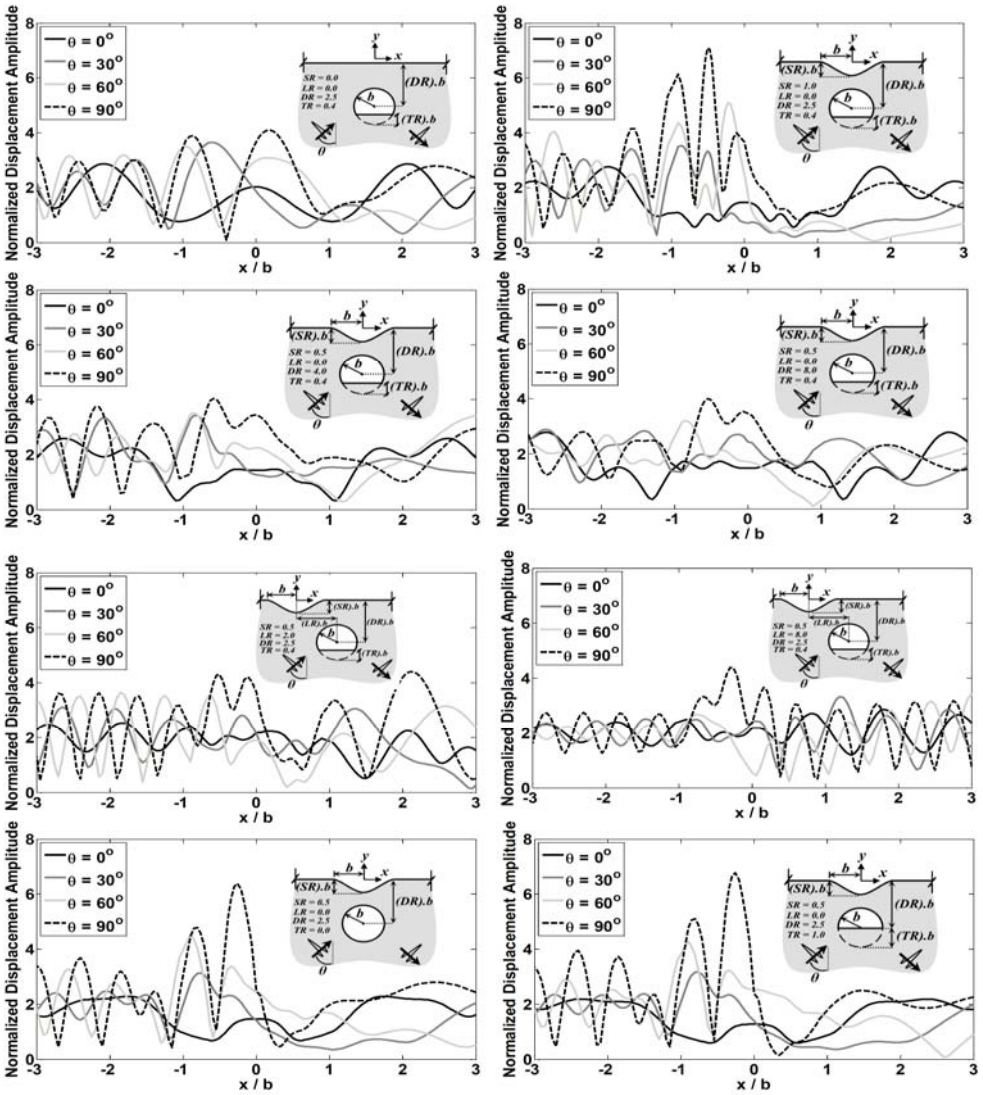

Fig. 11 The effect of the wave angle (θ) on the normalized displacement amplitude of the ground surface in two cases of the model geometric parameters

8. Conclusions

The behavior of the ground surface was shown in the presence of a semi-sine shaped valley above an embedded truncated circular cavity due to obliquely propagating incident antiplane waves as the Ricker wavelets type. An extensive time-domain half-plane BEM formulation was considered for this numerical study. The accuracy and efficiency of the prepared algorithm in antiplane seismic analysis of combined topographic problems were investigated and verified with those of excellent analytical works. First, general pattern of the responses in the time and frequency domain was observed. Then, with considering four geometric ratios of the model such as shape ratio, depth ratio, location ratio and truncation ratio as well as incident wave angle, a parametric study was carried out. The obtained results were summarized as follows:

1. The existence of valley decreased responses in case of vertically propagating waves compared to the smooth ground with a subsurface cavity.
2. Increasing the depth of the cavity decreased its seismic isolation effect in the case of vertical incident waves.
3. That side of the valley which was close to the cavity location experienced more fluctuations and another side converged rapidly to ground response without subsurface openings.
4. Although varying the cavity section from full-circle to semi-circle had significant influence on its surrounding stresses, the antiplane seismic response did not highly depend on truncation thickness ratio.
5. In spite of the fact that vertical incident waves created critical states in the case of single hill or valley structures, the highest response amplitude in the presence of underground cavities observed in horizontally propagating incident waves.

It is worth mentioning that, according to the purpose of

this paper which focused on the observation of the effect of model geometric parameters, the results were presented at a single frequency. Considering the frequency content can be also significant, which was not discussed in the present study.

Whereas the model presented in this paper showed some advantages of the half-plane time domain BEM, it is obvious that the mentioned method had also some important limitations. Seismic analysis of non-homogenous mediums with the half-plane BEM was not so straightforward. Besides, they could not be simply extended to important cases such as anisotropic and viscoelastic media.

References

[1] Panji M, Kamalian M, Asgari Marnani J, Jafari M.K. The Literature Review of Seismic Analysis of Topographic Features Subjected to Incident *SH*-waves, IIEES Research Bulletin, 2013a, No. 4, Vol. 15, pp. 1-15.

[2] Lee V.W, Trifunac M.D. Response of Tunnels to Incident SH-waves, Journal of the Engineering Mechanics Division, ASCE, 1979, No. EM4, Vol. 105, pp. 643-659.

[3] Datta S.K, Shah A.H. Scattering of SH Waves by Embedded Cavities, Wave Motion, No. 3, Vol. 4, 1982, 4, pp. 265-283.

[4] Manoogian M.E, Lee V.W. Diffraction of SH-waves by Subsurface Inclusions of Arbitrary Shape, Journal of Engineering Mechanics, ASCE, 1996, No. 2, Vol. 122, pp. 123-129.

[5] Manoogian M.E. Scattering and Diffraction of SH Waves above an Arbitrarily Shaped Tunnel, ISET Journal of Earthquake Technology, 2000, Nos. 1-3, Vol. 37, pp. 11-26.

[6] Lee V.W, Chen S, Hsu I.R. Antiplane Diffraction from Canyon above Subsurface Unlined Tunnel, Journal of Engineering Mechanics, ASCE, 1999, No. 6, Vol. 125, pp. 668-675.

[7] Smerzini C, Aviles J, Paolucci R, Sanchez-Sesma F.J. Effect of Underground Cavities on Surface Earthquake Ground Motion under SH Wave Propagation, Earthquake Engineering and Structural Dynamics, 2009, No. 12, Vol. 38, pp. 1441-1460.

[8] Tsaur D, Chang K. Multiple Scattering of SH Waves by an Embedded Truncated Circular Cavity, Journal of Marine Science and Technology, 2012, No. 1, Vol. 20, pp. 73-81.

[9] Beskos D.E. Boundary Element Methods in Dynamic Analysis, Applied Mechanics Review, 1987, No. 1, Vol. 40, pp. 1-23.

[10] Beskos D.E. Boundary Element Methods in Dynamic Analysis: Part II (1986-1996), Applied Mechanics Review, 1997, No. 3, Vol. 50, pp. 149-197.

[11] Friedman M.B, Shaw R. Diffraction of Pulses by Cylindrical Obstacles of Arbitrary Cross Section, Journal of Applied Mechanics, 1962, No. 1, Vol. 29, pp. 40-46.

[12] Mansur W.J, Brebbia C.A. Formulation of the Boundary Element Method for Transient Problems Governed by the Scalar Wave Equation, Applied Mathematical Modeling, 1982, No. 4, Vol. 6, pp. 307-311.

[13] Mansur W.J. A Time-stepping Technique to Solve Wave Propagation Problems using the Boundary Element Method, Ph.D. Dissertation, University of Southampton, 1983.

[14] Dominguez J. Boundary Elements in Dynamics, Computational Mechanics Publications, Southampton, Boston, 1993.

[15] Israil A.S.M, Banerjee P.K. Advanced Development of Time-domain BEM for Two-Dimensional Scalar Wave Propagation, International Journal for Numerical Methods in Engineering, 1990, No. 5, Vol. 29, pp. 1003-1020.

[16] Kamalian M, Gatmiri B, Sohrabi-Bidar A. On Time-domain Two-dimensional Site Response Analysis of Topographic Structures by BEM, Journal of Seismology and Earthquake Engineering, 2003, No. 2, Vol. 5, pp. 35-45.

[17] Yu G, Mansur W.J, Carrer J.A.M, Gong L. Stability of Galerkin and Collocation Time Domain Boundary Element Methods as Applied to the Scalar Wave Equation, Computers and Structures, 2000, No. 4, Vol. 74, pp. 495-506.

[18] Soares Jr. D, Mansur W.J. An Efficient Time-truncated Boundary Element Formulation Applied to the Solution of the Two-Dimensional Scalar Wave Equation, Engineering Analysis with Boundary Elements, 2009, No. 1, Vol. 33, pp. 43-53.

[19] Ahmad S, Banerjee P.K. Multi-domain BEM for Two-dimensional Problems of Elastodynamics, International Journal for Numerical Methods in Engineering, 1988, No. 4, Vol. 26, pp. 891-911.

[20] Sanchez-Sesma F.J, Campillo M. Diffraction of P, SV, and Rayleigh Waves by Topographic Features: a Boundary Integral Formulation, Bulletin of the Seismological Society of America, 1991, No. 6, Vol. 81, pp. 2234-2253.

[21] Dravinski M. Scattering of Waves by a Sedimentary Basin with a Corrugated Interface. Bulletin of the Seismological Society of America, 2007, No. 1B, Vol. 97, pp. 256-264.

[22] Yu M.C, Dravinski M. Scattering of a Plane Harmonic SH Wave by a Completely Embedded Corrugated Scatterer, International Journal for Numerical Methods in Engineering, 2009, No. 2, Vol. 78, pp. 196-214.

[23] Takemia H, Fujiwara A. SH-wave Scattering and Propagation Analysis at Irregular Sites by Time-domain BEM, Bulletin of the Seismological Society of America, 1994, No. 5, Vol. 84, pp. 1443-1455.

[24] Kamalian M, Jafari M.K, Sohrabi-Bidar A, Razmkhah A, Gatmiri B. Time-domain Two-dimensional Site Response Analysis of Non-homogeneous Topographic Structures by a Hybrid FE/BE Method, Soil Dynamics and Earthquake Engineering, 2006, No. 8, Vol. 26, pp. 753-765.

[25] Kamalian M, Gatmiri B, Sohrabi-Bidar A, Khalaj A. Amplification Pattern of 2D Semi-sine Shaped Valleys Subjected to Vertically Propagating Incident Waves, Communication in Numerical Methods in Engineering, 2007, No. 10, Vol. 23, pp. 871– 887.

[26] Kamalian M, Jafari M.K, Sohrabi-Bidar A, Razmkhah A. Seismic Response of 2D Semi-sine Shaped Hills to Vertically Propagating Incident Waves: Amplification Patterns and Engineering Applications, Earthquake Spectra, 2008a, No. 2, Vol. 24, pp. 405-430.

[27] Kamalian M, Sohrabi-Bidar A, Razmkhah A, Taghavi A, Rahmani I. Considerations on Seismic Microzonation in Areas with Two-dimensional Hills, Journal of Earth System Science, 2008b, No. 2, Vol. 117, pp. 783–796.

[28] Alielahi H, Kamalian M, Asgari Marnani J, Jafari M.K, Panji M. Applying a Time-domain Boundary Element Method for Study of Seismic Ground Response in the Vicinity of Embedded Cylindrical Cavity, International Journal of Civil Engineering, In press, 2013.

[29] Dominguez J, Meise T. On the Use of the BEM for Wave Propagation in Infinite Domains, Engineering Analysis with Boundary Elements, 1991, No. 3, Vol. 8, pp. 132-138.

[30] Wong H.L, Jennings P.C. Effects of Canyon Topography on Strong Ground Motion, Bulletin of the Seismological Society of America, 1975, No. 5, Vol. 65, pp. 1239-1257.
[31] Sanchez-Sesma F.J, Rosenblueth E. Ground Motion at Canyons of Arbitrary Shape under Incident SH Waves, Earthquake Engineering and Structural Dynamics, 1979, No. 5, Vol. 7, pp. 441-450.
[32] Ohtsu M, Uesugi S. Analysis of SH Wave Scattering in a Half Space and its Applications to Seismic Responses of Geological Structures, Engineering Analysis, 1985, No. 4, Vol. 2, pp. 198-204.
[33] Reinoso E, Wrobel L.C, Power H. Preliminary Results of the Modeling of the Mexico City Valley with a Two-dimensional Boundary Element Method for the Scattering of SH Waves, Soil Dynamics and Earthquake Engineering, 1993, No. 8, Vol. 12, pp. 457-468.
[34] Ausilio E, Conte E, Dente G. Seismic Response of Alluvial Valleys to SH Waves, Seismic Engineering Conference, AIP Conference Proceedings, 2008, Vol. 1020, pp. 199-206.
[35] Benites R, Aki K, Yomogida K. Multiple Scattering of SH Waves in 2-D Media with Many Cavities, Pure and Applied Geophysics, 1992, No. 3, Vol. 138, pp. 353-390.
[36] Hirai H. Analysis of Transient Response of SH Wave Scattering in a Half-space by the Boundary Element Method, Engineering Analysis, 1988, No. 4, Vol. 5, pp. 189-194.
[37] Belytschko T, Chang H.S. Simplified Direct Time Integration Boundary Element Method, Journal of Engineering Mechanics, ASCE, 1988, No. 1, Vol. 114, pp. 117-134.
[38] Panji M, Kamalian M, Asgari Marnani J, Jafari M.K. Transient Analysis of Wave Propagation Problems by Half-plane BEM, Geophysical Journal International, No. 3, Vol. 194, pp. 1849-1865.
[39] Eringen A.C, Suhubi E.S. Elastodynamics, Academic Press, New York, 1975.
[40] Kawase H. Time-domain Response of a Semi-circular Canyon for Incident SV, P, and Rayleigh Waves Calculated by the Discrete Wavenumber Boundary Element Method, Bulletin of the Seismological Society of America, 1988, No. 4, Vol. 78, pp. 1415-1437.
[41] Brebbia C.A, Dominguez J. Boundary Elements, an Introductory Course, Computational Mechanics Publications, Southampton, Boston, 1989.
[42] Hadley P.K, Askar A, Cakmak A.S. Scattering of Waves by Inclusions in a Non-homogeneous Elastic Half Space Solved by Boundary Element Methods, Technical Report NCEER-89-0027, 1989.
[43] Ricker N, The Form and Laws of Propagation of Seismic Wavelets, Geophysics, 1953, No. 1, Vol. 18, pp. 10-40.
[44] Koyama Y. Present status and technology of shield tunneling method in Japan, Tunneling and Underground Space Technology, 2003, Vol. 18, pp. 145-159.
[45] Sanchez-Sesma F.J, Campillo M, Irikura K. A Note on the Rayleigh Hypothesis and the Aki-Larner Method, Bulletin of the Seismological Society of America, 1989, No. 6, Vol. 79, pp. 1995-1999.
[46] Trifunac M.D. Scattering of Plane SH Waves by a Semi-cylindrical Canyon, Earthquake Engineering and Structural Dynamics, 1973, No. 3, Vol. 1, pp. 267-281.